A simplified cell-based assay to identify coronavirus 3CL protease inhibitors

Samuel J. Resnick[1,2], Sho Iketani[3,4], Seo Jung Hong[1], Arie Zask[5], Hengrui Liu[6], Sungsoo Kim[1], Schuyler Melore[1], Manoj S. Nair[3], Yaoxing Huang[3], Nicholas E.S. Tay[6], Tomislav Rovis[6], Hee Won Yang[1], Brent R. Stockwell[5,6*], David D. Ho[3*], Alejandro Chavez[1*]

[1] Department of Pathology and Cell Biology, Columbia University Irving Medical Center, New York, NY, 10032, USA

[2] Medical Scientist Training Program, Columbia University Irving Medical Center, New York, NY, 10032, USA

[3] Aaron Diamond AIDS Research Center, Columbia University Irving Medical Center, New York, NY, 10032, USA

[4] Department of Microbiology and Immunology, Columbia University Irving Medical Center, New York, NY, 10032, USA

[5] Department of Biological Sciences, Columbia University, New York, NY, 10027, USA

[6] Department of Chemistry, Columbia University, New York, NY, 10027, USA

***Correspondence to: ac4304@cumc.columbia.edu; dh2994@cumc.columbia.edu; bstockwell@columbia.edu**

Abstract

We describe a mammalian cell-based assay capable of identifying coronavirus 3CL protease (3CLpro) inhibitors without requiring the use of live virus. By enabling the facile testing of compounds across a range of coronavirus 3CLpro enzymes, including the one from SARS-CoV-2, we are able to quickly identify compounds with broad or narrow spectra of activity. We further demonstrate the utility of our approach by performing a curated compound screen along with structure-activity profiling of a series of small molecules to identify compounds with antiviral activity. Throughout these studies, we observed concordance between data emerging from this assay and from live virus assays. By democratizing the testing of 3CL inhibitors to enable screening in the majority of laboratories rather than the few with extensive biosafety infrastructure, we hope to expedite the search for coronavirus 3CL protease inhibitors, to address the current epidemic and future ones that will inevitably arise.

Introduction

The outbreak of a novel coronavirus (SARS-CoV-2) infection of the past several months has paralyzed countries around the world[1,2]. This crisis is further exacerbated by the dearth of approved therapeutics, leaving physicians with few proven treatment options. In the past two decades, the world has already suffered from two other major coronavirus outbreaks, Severe Acute Respiratory Syndrome (SARS) and Middle East Respiratory Syndrome (MERS), suggesting that coronaviruses represent a real and ever-present threat to global health that must be addressed[3]. Yet, even if therapeutics against the existing epidemic strains are identified, there are several hundred other coronaviruses in active circulation within animal populations, many with the theoretical potential to infect humans. To help identify therapeutics for the current epidemic along with preparing for the next, there is a need for readily deployable small molecule screening assays that enable the identification of therapeutics that are broad-acting across a large collection of coronavirus strains.

During coronavirus infection, the RNA genome is delivered into cells and translated into a pair of polyproteins[4]. These polyproteins are then processed by a set of virally encoded proteases, of which the three-chymotrypsin-like protease (3CLpro) performs the majority of cleavage events[4]. As a result of its essential role in viral replication and high degree of conservation across all coronaviruses, 3CLpro enzymes represent important targets for therapeutic drug development[5,6]. Previous work expressing a variety of viral proteases within yeast and mammalian cellular systems have shown that protease expression can lead to profound cellular toxicity, which can be rescued by the addition of protease inhibitors[7–12]. We hypothesized that if the expression of coronavirus 3CLpro enzymes within mammalian cells leads to a similar toxic phenotype, this could form the basis of an easily implemented mammalian cell-based assay to evaluate protease inhibitors. While multiple assays exist to evaluate protease inhibitors, an assay of the nature we envisioned has clear advantages, as it requires minimal upfront cost or effort, is accessible to many biomedical research labs, does not involve the use of live virus, and requires no specialized reporter to read out protease activity. In contrast, *in vitro* protease assays using purified protein have formed the backbone of inhibitor

screening, but require upfront efforts to isolate the pure protease and are not conducted under physiologic cellular conditions[13,14]. In addition, if one desires to identify broad-acting coronavirus inhibitors, one must purify and identify experimental conditions suitable for testing each protease *in vitro*. An alternative approach for identifying protease inhibitors is the use of live virus which is performed under more biologically relevant conditions, assuming relevant host cell systems can be identified, but requires intensive safety training and specialized biosafety protocols[15]. For many coronaviruses, no live virus assay exists, limiting the ability to test compounds within mammalian cell systems to a small subset of all coronaviruses[16]. Furthermore, compounds with activity against live virus may function through a number of mechanisms other than protease inhibition which cannot be readily determined, and may lead to undesired off-target activities which are not realized until much later in the drug development process[17,18].

Here, we report a mammalian cell-based assay to identify coronavirus 3CLpro inhibitors that does not require the use of live virus. We demonstrate the utility of the assay using the SARS-CoV-2 3CLpro, with EC_{50} values obtained from the assay showing good concordance with traditional live virus testing for multiple compounds. We next establish the generality of the approach by testing a diverse set of 3CLpro enzymes. Finally, we perform a small molecule screen, along with structure-activity profiling of a set of compounds to find those with enhanced antiviral activity. The presented data support the use of our assay system for the discovery of small molecule 3CLpro inhibitors and the rapid characterization of their activity across multiple coronaviruses to identify those with broad inhibitory activity.

Results

Expression of the SARS-CoV-2 3CLpro in HEK293T cells results in cell toxicity and can be used as a readout of drug activity

Prior work has shown that the exogenous expression of viral proteases within cellular systems can result in growth suppression or cell death. Motivated by this work, we sought to determine the effect of expressing the SARS-CoV-2 3CLpro in HEK293T cells. Utilizing a cost-effective crystal-violet-based approach to quantify cell abundance, we observed that expression of SARS-CoV-2 3CLpro results in significant growth inhibition as compared to the expression of a control protein, enhanced yellow fluorescent protein (EYFP) (Fig. 1a-b)[19]. This suppression of growth was dependent upon the catalytic function of the enzyme, as mutating cysteine 145, which is essential for the enzyme's peptidase activity, abolished the growth defect (Fig. 1a-b). We sought to determine if the observed growth defect could be rescued by incubating cells with GC376, a feline coronavirus inhibitor that was recently reported to have activity against SARS-CoV-2 3CLpro[20]. In comparison to untreated control cells, the addition of GC376 led to a robust increase in cell growth (Fig. 1c-d).

Compound rescue of transfected 3CLpro cytotoxicity is similar to results obtained with live virus

We next tested if this transfection-based assay could be used to determine compound EC_{50} values and whether the values showed any correlation with those obtained with live virus. After incubating SARS-CoV-2 3CLpro transfected cells with a range of GC376 concentrations, we calculated an EC_{50} of 3.30 μM, which is similar to published values reported using live virus on Vero E6 (EC_{50} 2.2 μM, 0.9 μM, 0.18 μM, 4.48 μM) and Vero 76 cells (EC_{50} 3.37 μM) (Fig. 2a and Table 1)[20–24]. We investigated the assay's tolerance to deviation by varying the amount of plasmid transfected or the number of cells seeded into wells containing compound (Supplementary Fig. 1). In all cases, the assay was robust to variation, delivering a similar EC_{50} for GC376 across all conditions. We also tested an orthogonal method of quantifying cell abundance based on fluorescence microscopy and observed agreement with the results obtained with crystal violet staining (Supplementary Fig. 2). This suggests that the assay system is robust to variation and provides consistent results.

We next conducted dose-response profiling for two additional SARS-CoV-2 3CLpro inhibitors, compound 4 and compound 11a, and observed reversal of the toxic effect of the protease in a dose-dependent manner (Fig. 2b-c)[25,26]. In agreement with the results obtained with GC376, the EC_{50} value for compound 4 was comparable to those obtained with live virus, 0.98 μM and 3.023 μM, respectively (Table 1)[24]. Unexpectedly, we calculated an EC_{50} of 6.89 μM for 11a, which is approximately 10-fold higher than the literature reported value of 0.53 μM, based on viral plaque assay[26]. We have noticed that literature reported EC_{50} values from live virus testing could range over an order of magnitude depending on the exact method employed, as is the case for GC376 (Table 1). To resolve this discrepancy between the transfection-based approach and the live virus assay, we conducted live virus testing of 11a using the commonly employed readout of cytopathic effect in Vero E6 cells and observed closer concordance with our transfection-based results (Supplementary Figure 3 and Table 1)[20,24,27]. To measure the toxicity of each compound, we exposed EYFP-transfected cells to each molecule and determined CC_{50} values (Fig. 2). We also calculated the selectivity index (SI) for each compound tested in this study (Supplementary Table 1).

We hypothesized that the assay would be able to distinguish between compounds that are only active on the purified SARS-CoV-2 3CLpro and those that are able to inhibit the live virus through protease inhibition. In general, we observe concordance between compounds showing activity within this transfection-based 3CL assay and live virus studies (Supplementary Fig. 4a-e)[13]. However, within the assay, we did not observe activity for ebselen, a small molecule with demonstrated activity against the SARS-CoV-2 3CLpro *in vitro* and activity against the SARS-CoV-2 live virus (Supplementary Fig. 4f). We suggest that this may be due to ebselen targeting more than 3CLpro within the live virus assay, which is in line with work showing that ebselen is highly reactive and readily forms selenosulfide bonds with numerous proteins including the SARS-CoV-2 papain-like protease (PLP)[18,28,29].

Demonstrating assay compatibility across a range of coronavirus 3CLpro enzymes

We hypothesized that this assay may be used to study other coronavirus 3CLpros to enable users to identify broad-acting inhibitors, as constructs containing other 3CLpro enzymes could be readily synthesized. To test the assay's generality, we created expression constructs for 3CL proteases from five other coronaviruses (SARS-CoV, MERS-CoV, Bat-CoV-HKU9, HCoV-NL63 and IBV) with variable amino acid identity compared with SARS-CoV-2 3CLpro (Supplementary Fig. 5a). For each of these proteases, we confirmed that expression in mammalian cells resulted in toxicity that is dependent upon the enzyme's catalytic activity (Supplementary Fig. 5b). Next, we tested GC376, compound 4, and 11a across this panel of proteases. GC376, a drug originally identified for use against the Feline Infectious Peritonitis virus, showed EC_{50} <10 μM for the most, but not all of proteases tested[30]. Unexpectedly, compound 4, which was originally designed as a SARS-CoV 3CLpro inhibitor showed particular potency against IBV 3CLpro (EC_{50} = 0.058 μM) along with broad activity (EC_{50} <10 μM) for all other 3CL proteases tested. In contrast to GC376 and compound 4, 11a had a relatively narrow activity spectrum with EC_{50} <10 μM against only SARS-CoV and SARS-CoV-2 3CLpro enzymes (Fig. 3). Of note, in all cases where previous live virus data was available, the EC_{50} values obtained from this transfection-based assay were similar (Table 1).

Rapid testing to identify SARS-CoV-2-3CL protease inhibitors

Having further determined the assay's ability to examine the effects of active individual compounds, we sought to determine its suitability for small molecule screening. Before performing the screen, we optimized the testing parameters to ensure suitable performance characteristics (Supplementary Fig. 6 and Methods)[31]. We compiled a collection of 162 diverse protease inhibitors, along with compounds with reported *in vitro* activity against 3CLpro enzymes or structural similarity to known 3CLpro inhibitors (Supplementary Table 2 and Supplementary Table 3). Of the nearly 200 compounds tested, two potent hits were identified, GC373 and GRL-0496 (Fig. 4a, Supplementary Table 2)[32].

We noted that GC373 is structurally similar to its prodrug GC376, except for the change of the bisulfide salt adduct to an aldehyde warhead[22,33]. Additional testing of GC373 revealed it to have a similar EC_{50} as GC376 in both the transfection assay and when tested against live SARS-CoV-2 virus, suggesting that the differences in structure has a minimal effect on their potency (Supplementary Fig. 7 and Table 1), although solubility may be affected[33]. The other hit from the screen, GRL-0496, shares structural similarity to several other compounds within the library, one of which is a previously reported 3CLpro inhibitor (MAC-5576) that failed to show activity against SARS-CoV-2 in a live virus assay[24,34]. Additional testing of GRL-0496 revealed it to have an EC_{50} of 5.05 μM against SARS-CoV-2 3CLpro within our transfection-based assay (Fig. 4c). To verify GRL-0496's activity, we tested it against live SARS-CoV-2 virus, and confirmed its potency (EC_{50} = 9.12 μM) (Fig. 4d). We next tested GRL-0496 against the full panel of 3CLpro enzymes we had previously examined and observed a narrow range of activity, with EC_{50} <10 μM only observed against SARS-CoV 3CLpro and SARS-CoV-2 3CLpro, in agreement with previous live virus testing (Supplementary Fig. 8 and Table 1)[27]. We also tested GC373 against the full panel of 3CLpro enzymes and observed concordance with GC376, with SARS-CoV 3CLpro, MERS-CoV 3CL pro, and IBV 3CL pro demonstrating an EC_{50} <10 μM (Supplementary Fig. 8).

Discussion

Given the potential for protease inhibitors in the treatment of viral illnesses, small molecule inhibitors of coronavirus 3CL proteases represent a promising avenue for treating infections caused by this large family of viruses. Here, we present a simplified assay to identify candidate inhibitors under physiologic cellular conditions. This approach presents significant advantages over other methods to detect 3CL protease inhibitory activity with its ease of use and ability to be performed with equipment and reagents commonly available to many biomedical research laboratories. While conventional methods for identifying 3CL protease inhibitors make use of *in vitro* purified protease, the isolation of sufficiently pure enzyme in its native state can be costly and labor intensive. Furthermore, assays using purified protease fail to consider cell permeability and the influence of the extracellular and

intracellular milieu on compound activity. In comparison to live virus-based assays, the outlined approach does not require extensive biosafety containment. These data also suggest that the approach described here is applicable to a number of coronaviruses for which live virus assays may not be available or would be deemed ethically challenging to be performed even with extensive biosafety infrastructure[35,36]. Finally, because the phenotype assayed within this approach is driven solely by protease activity, it may enable the distinction between compounds with multiple biological targets and subsequent potential for off-target toxicity from those that function primarily as 3CLpro inhibitors.

A number of surrogate assays that aim to identify molecules with activity against proteins encoded by SARS-CoV-2 have recently been reported[37–39]. These assays were developed to provide physiologically meaningful molecule testing without needing to use live SARS-CoV-2 cultures in order to allow for rapid testing and widespread adoption to labs without necessary safety infrastructure. The aforementioned assays have focused primarily on identifying neutralizing antibodies targeted at the SARS-CoV-2 spike (S) protein. To our knowledge, a reporter-free surrogate assay to identify coronavirus 3CL protease inhibitors validated with multiple known coronavirus 3CL protease inhibitors has not been reported.

Within the literature, EC_{50} values obtained for a 3CLpro inhibitor against live virus can show a broad range of potency, with some compounds demonstrating EC_{50} values across multiple orders of magnitude (Table 1). These differences appear to be driven by variation in experimental setup such as cell line used, assay readout, incubation period, and initial concentration of virus added. While we have observed agreement between the EC_{50} values obtained from the described transfection-based method and those reported in the literature, given the differences in EC_{50} across assays, we suggest caution when comparing results across studies. By developing this transfection-based 3CLpro testing platform, we hope to facilitate the discovery of new coronavirus inhibitors while also facilitating the comparison of existing inhibitors within a single simplified assay system. Furthermore,

we propose that this cellular protease assay system could be industrialized to screen and optimize a large number of compounds to discover potential treatments for future viral pandemics.

Methods

Cell Lines and Cell Culture

HEK293T and HEK293 cells used in this study were obtained from ATCC. Cells were maintained at 37°C in a humidified atmosphere with 5% CO_2. HEK293T and HEK293 cells were grown in Dulbecco's Modified Eagle Medium (DMEM, Invitrogen) which was supplemented with 10% fetal bovine serum (Gibco) and penicillin-streptomycin (Invitrogen). HEK293T and HEK293 cells were confirmed to be free of mycoplasma contamination with the Agilent MycoSensor PCR Assay Kit. To obtain HEK293 cells stably expressing EYFP, cells were co-transfected with EYFP plasmids harboring the *piggyBac* transposon (pPB bsr2-EYFP) (Yusa et al., 2009) and pCMV-mPBase (mammalian codon-optimized PBase) encoding a piggyBac transposase using Lipofectamine 2000 (Invitrogen) according to the manufacturer's instructions. One day after transfection, the transfected cells were selected with 10 µg/mL of blasticidin (Invitrogen).

Transfections and Drug Selections

24 h prior to transfection, 293T cells were seeded at 65-75% confluency into 24-well plates coated for 30 min with a 1 mg/mL solution of poly-D-lysine (MP Biomedicals Inc.) and washed with PBS (Gibco) once prior to media addition. The next day, 500 ng of 3CLpro expression plasmid, unless otherwise stated, was incubated with Opti-MEM and Lipofectamine 2000 for 30 min at room temperature prior to dribbling on cells, as per manufacturer's protocol. For plating into drug conditions, 20 h after transfection, cells were washed once with PBS and 200 µL Trypsin-EDTA 0.25% (Gibco) was added to cells to release them from the plate. Trypsinized cell slurry was pipetted up and down repeatedly to ensure a single cell suspension. 96-well plates were coated with poly-D-lysine, either coated manually with 1 µg/mL poly-D-lysine in PBS solution for 30 min or purchased pre-coated with poly-D-lysine (Corning). Wells were filled with 100 µL of media ± drug and 1 µg/mL

puromycin and were seeded with 9 µL of trypsinized cell slurry. For higher throughput experiments, multiple individually transfected wells of a 24-well plate were combined after trypsinization and prior to seeding in drug. After seeding into wells containing drug and puromycin, cells were incubated for 48 h unless otherwise specified.

Plasmids

All vectors used in this study were cloned into the pLEX307 backbone (Addgene #41392) using Gateway LR II Clonase Enzyme mix (Invitrogen). 3CL proteases used in this study were generated using gene fragments ordered from Twist Biosciences. Inactive 3CL proteases were generated by site directed mutagenesis of the essential catalytic cysteine. DNA was transformed into NEB 10-beta high efficiency competent cells. Sanger sequencing to verify proper inserts were done for all plasmids used in this study (Genewiz).

Plasmid DNA was isolated using standard miniprep buffers (Omega Biotek) and silica membrane columns (Biobasic). To reduce batch-to-batch variability between plasmid DNA isolations and its subsequent impact on transfection efficiency, multiple plasmid DNA extractions were conducted in parallel, diluted to 50 ng/µL and pooled together.

Crystal Violet Staining and Quantification

The crystal violet staining protocol was adapted from Feoktistova et. al.[19] Briefly, after compound incubation with 3CLpro expressing cells in 96-well plates, the medium was discarded and cells were washed once with PBS. Cells were incubated with 50 µL of crystal violet staining solution (0.5% crystal violet in 80% water and 20% methanol) and rocked gently for 30 min. The staining solution was removed and cells were washed four times with water using a multichannel pipette. Stained cells were left to dry for ≥4 h on the laboratory bench or within the chemical hood. The crystal violet staining solution was eluted by the addition of 200 µL of methanol over the course of 30 min with gentle rocking. Plates were sealed with parafilm to mitigate methanol evaporation. 100 µL of eluted

stain from each well was transferred to a new 96-well plate for reading in a Tecan Infinite F50 plate reader. Absorbance was measured at 595 nm twice and values were averaged between replicate measurements. Blank wells were included in each batch of experiments, and absorbance values were normalized by background levels of staining from blank wells.

Statistical Analysis of Dose Response Curves

For analysis of crystal violet staining experiments, relative growth was calculated from background normalized absorbance values. Test wells containing drug were divided by average background normalized values from wells where cells were expressing protease and exposed to vehicle, when available. Otherwise, values were normalized by values from protease-expressing cells exposed to the lowest concentration of drug included in the dose-response curve. When there were significant deviations from protease-expressing cells exposed to no drug and protease-expressing cells exposed to lowest concentrations of drug included in the dose-response curve, experiments were repeated with normalization by protease-expressing cells exposed to no drug. CC_{50} values were calculated in Prism using the nonlinear regression functionality and derived from dose-response curves with EYFP transfected cells. A nonlinear curve fitting function accounting for variable curve slopes was calculated by plotting the normalized response as a function of log(compound). Similarly, EC_{50} values were calculated in GraphPad Prism also using the nonlinear regression functionality. A nonlinear curve fitting function measuring the stimulatory response of a compound as a function of an unnormalized response was used to calculate the EC_{50}. All reported values were confirmed to not have ambiguous curve fitting. The 95% confidence interval of EC_{50} calculations was also calculated and included.

For analysis of live virus experiments, EC_{50} values were determined by fitting a nonlinear curve to the data with the assumption of a normalized response (GraphPad Prism). Cells were confirmed as mycoplasma negative prior to use.

Compound Screening

For screening condition optimization, we measured the Z-Factor for replicates of positive controls GC376, tested at 50 μM, and compound 4, tested at 20 μM. Replicate measurements were recorded for DMSO negative controls and positive control compounds after 48, 72, and 96 h of incubation with drug. Background normalized crystal violet absorbance values at each timepoint were collected.

During the drug screen, within each of the four plates screened, two positive controls wells were included to ensure assay reliability, along with several wells with the negative control 0.1% DMSO condition. All compounds were screened at 10 μM resuspended in DMSO (Fisher Scientific).
For hit selection, we employed a robust z-score method. We first normalized data using a robust z-score that uses median and median absolute deviation (MAD) instead of mean and standard deviation. We then used a threshold of 3.5 MAD to determine which drugs rescued the cytotoxicity imposed by expression of the viral protease[40].

Live Virus Assay

The SARS-CoV-2 strain 2019-nCoV/USA_WA1/2020 was grown and titered in Vero-E6 cells. One day before the experiment, Vero-E6 cells were seeded at 30,000 cells/well in 96 well-plates. Serial dilutions of the test compound were prepared in media (EMEM + 10% FCS + penicillin/streptomycin), pipetted onto cells, and virus was subsequently added to each well at an MOI of 0.2. Cells were incubated at in a humidified environment at 37 °C with 5% CO_2 for 72 h after addition of virus. Cytopathic effect was scored by independent, blinded researchers. The reported cytopathic effect value represents the average from two independent reviewers. Percent Inhibition was calculated by comparison to control wells with no inhibitor added. All live virus experiments were conducted in a biosafety level 3 lab.

Microscopy

Cells plated on a 96-well plate (Greiner Bio-OneTM) and washed once immediately before imaging. EYFP fluorescence imaging was performed using an Axio Observer 7 microscope (Zeiss) equipped with a Plan-Apochromat 10X objective (0.45 N.A.) with 1-by-1 pixel binning. Optical Illumination bias was empirically derived by sampling background areas and subsequently used to flatten images. After a global background subtraction, cell density was calculated based on area of EYFP intensity.

Compounds and Chemical Synthesis

GC376 was purchased from Aobious. Myrecetin, rupintrivir, grazoprevir, saquinavir, fosamprenavir, indinavir, apigenin, quercetin, famotidine, MDL28170, bicailein, betrixaban, and amentoflavone were purchased from Fisher Scientific. Tipranavir was purchased from Cayman Chemical. MAC5576, MAC22272, MAC8120, MAC30731, BTB07404, BTB07408, MWP00332, BTB07417, MWP00508, MWP00333, BTB07407, SPB08384, SPB06613, SPB06636, SPB06591, SPB06593, MWP00709, CC42746, BTB07789, BTB07420, MWP00710, BTB07421, SCR00533, and SEW03089 were purchased from Maybridge. GRL-0496 and GRL-0617 were purchased from Focus Biomolecules. AZVIII-40A (1,2-Benzisothiazol-3(2*H*)-one) was purchased from Alfa Aesar. Other protease inhibitors in table below were purchased from TargetMol.

CAS Number	Drug Name	CAS Number	Drug Name
1226781-44-7	Omarigliptin	134381-21-8	Epoxomicin
79183-19-0	Apoptosis Activator 2	110044-82-1	MG101
3731-52-0	Picolamine	125697-93-0	lavendustin C
541-91-3	Muscone	729607-74-3	BMS707035
60-23-1	2-Aminoethanethiol	630420-16-5	Asunaprevir
51146-56-6	Dexibuprofen	76684-89-4	Loxistatin Acid
3416-24-8	Glucosamine	1025015-40-0	GK921
56974-61-9	Gabexate mesylate	292632-98-5	L-685,458
7481-89-2	Zalcitabine	202138-50-9	Tenofovir Disoproxil Fumarate
2016-88-8	Amiloride hydrochloride	937174-76-0	GSK690693
945667-22-1	Saxagliptin hydrate	1256388-51-8	Ledipasvir
668270-12-0	Linagliptin	960374-59-8	ONX0914
486460-32-6	Sitagliptin	1401223-22-0	PI1840
136-77-6	Hexylresorcinol	13552-72-2	(+)-Isocorydine hydrochloride

497-76-7	Arbutin	697797-51-6	UAMC 00039 dihydrochloride
908-54-3	Diminazene Aceturate	1402727-29-0	PE859
6419-36-9	3-Pyridylacetic acid hydrochloride	847925-91-1	RO4929097
81110-73-8	Racecadotril	254750-02-2	Emricasan
50924-49-7	Mizoribine	161314-82-5	CGS 27023A
7414-83-7	Sodium etidronate	150080-09-4	Talabostat mesylate
103-16-2	Monobenzone	1441674-54-9	Ledipasvir acetone
1180-71-8	Limonin	130370-60-4	Batimastat
472-15-1	Betulinic acid	54857-86-2	TOFA
329-98-6	PMSF	1009734-33-1	HZ1157
42017-89-0	Fenofibric acid	188062-50-2	Abacavir sulfate
196597-26-9	Ramelteon	127373-66-4	Sivelestat
155213-67-5	Ritonavir	1132935-63-7	Dasabuvir
850649-62-6	Alogliptin Benzoate	20575-57-9	Calycosin
179324-69-7	Bortezomib	673-22-3	4-Methoxysalicylaldehyde
546-88-3	Acetohydroxamic acid	111-20-6	Sebacic acid
129618-40-2	Nevirapine	53936-56-4	Deoxyarbutin
192725-17-0	Lopinavir	490-78-8	2-5-dihydroxyacetophenone
39809-25-1	Penciclovir	29700-22-9	Oxyresveratrol
916170-19-9	AOB2796	88321-09-9	Aloxistatin
176161-24-3	Maribavir	864953-29-7	Fostemsavir
1029877-94-8	Trelagliptin succinate	519055-62-0	Tasisulam
1201902-80-8	MLN9708	425386-60-3	Semagacestat
354812-17-2	SC514	35943-35-2	Triciribine
1072833-77-2	Ixazomib	331862-41-0	IMR-1A
871038-72-1	Raltegravir potassium	310456-65-6	IMR1
863329-66-2	PSI6206	210344-98-2	Z-IETD-FMK
82009-34-5	Cilastatin	1624602-30-7	VR23
480-18-2	Taxifolin	161814-49-9	Amprenavir
82956-11-4	Nafamostat mesylate	1312782-34-5	AA26-9
1009119-65-6	Daclatasvir dihydrochloride	1051375-16-6	Dolutegravir
635728-49-3	Darunavir Ethanolate	1026785-59-0	Lomibuvir
142880-36-2	Ilomastat	112246-15-8	Ginsenoside Rh2
697761-98-1	Elvitegravir	256477-09-5	UK371804
1051375-19-9	Dolutegravir sodium	147859-80-1	CA-074 methyl ester
84687-43-4	Astragaloside IV	1404437-62-2	ML281
7770-78-7	Arctigenin	591778-68-6	CP 640186
83-48-7	Stigmasterol	5631-68-5	Hydroumbellic acid
478-01-3	Nobiletin	831-61-8	Ethyl gallate
34157-83-0	Celastrol	2469-34-3	Senegenin
29031-19-4	Glucosamine sulfate	28831-65-4	lithospermic acid

27409-30-9	Picroside I	209984-56-5	Dibenzazepine
848141-11-7	Alvelestat	209984-57-6	LY411575
128-53-0	N-Ethylmaleimide	1221573-85-8	Paritaprevir
208255-80-5	DAPT	1190307-88-0	Sofosbuvir
865759-25-7	Trelagliptin	1421438-81-4	Crenigacestat
187389-52-2	Z-VAD(OMe)-FMK	1338225-97-0	Doravirine
514-10-3	Abietic Acid	847499-27-8	Delanzomib
229975-97-7	Atazanavir sulfate	25406-64-8	Morroniside
136470-78-5	Abacavir	20633-67-4	Calycosin-7-O-beta-D-glucoside
354813-19-7	Balicatib	59870-68-7	Glabridin
868540-17-4	Carfilzomib	58749-22-7	Licochalcone A
198904-31-3	Atazanavir	1377049-84-7	Velpatasvir
274901-16-5	Vildagliptin	402957-28-2	Telaprevir
244767-67-7	Dapivirine	603139-19-1	Odanacatib
292605-14-2	SB-3CT	206361-99-1	Darunavir
179461-52-0	PD 151746	850876-88-9	Danoprevir
315183-21-2	PAC1	159989-65-8	Nelfinavir Mesylate
59721-29-8	Camostat mesilate	935888-69-0	Oprozomib
154598-52-4	Efavirenz	30827-99-7	AEBSF hydrochloride
1192224-24-0	Des(benzylpyridyl) Atazanavi	273404-37-8	Belnacasan
1194044-20-6	LY2811376	210344-95-9	Z-DEVD-FMK
313967-18-9	FLI06	197855-65-5	Z-FA-FMK
218156-96-8	SRPIN340	149488-17-5	Trovirdine
7497-07-6	NSC 405020	133407-82-6	MG132
103476-89-7	Leupeptin Hemisulfate	1051375-10-0	Cabotegravir
57-11-4	Stearic acid	1146699-66-2	Avagacestat

All other compounds used in the study were synthesized and quality checked according to the following protocols.

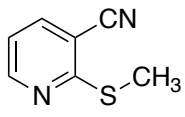

2-(methylthio)nicotinonitrile (xx-1) The title compound was prepared according to a published procedure; spectral data are in agreement with literature values[41].

^{1}H NMR (500 MHz, $CDCl_3$) δ 8.60 (dd, *J* = 5.0, 1.8 Hz, 1H), 7.79 (dd, *J* = 7.7, 1.8 Hz, 1H), 7.07 (dd, *J* = 7.7, 4.9 Hz, 1H), 2.64 (s, 3H).

^{13}C NMR (126 MHz, $CDCl_3$) δ 163.7, 152.2, 140.6, 118.4, 115.7, 107.5, 13.4.

HRMS High accuracy (ASAP): Calculated for $C_7H_6N_2S$ $(M+H)^+$: 151.0330; found: 151.0327.

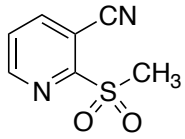

2-(methylsulfonyl)nicotinonitrile (xx-2) The title compound was prepared from xx-1 according to a modified procedure from the literature[42].

Pyridine xx-1 (87 mg, 0.58 mmol, 1 equiv) was weighed into 50 mL round bottom flask equipped with a stir bar. The solid was dissolved in 10 mL of anhydrous MeOH, followed by portion-wise (usually 3 portions) additions of mCPBA (500 mg, 2.9 mmol, 5 equiv). Substrate conversion was monitored via TLC analysis (70% EtOAc:Hex to 100% EtOAc), with up to an additional 5 equiv of mCPBA added if necessary. Upon complete conversion of starting material, the reaction was quenched with 20 mL of saturated aqueous $NaHCO_3$, diluted with an additional 20 mL of DCM. The layers were separated and the organic layer was further washed (2x) with 10 mL of of saturated aqueous $NaHCO_3$. The organic layer was then dried *in vacuo* and purified via silica gel column chromatography (100% EtOAc to 5% MeOH:EtOAc) to yield 51 mg (48% yield) of the desired sulfone as a white solid.

^{1}H NMR (400 MHz, $CDCl_3$) δ 8.86 (dd, *J* = 4.8, 1.6 Hz, 1H), 8.26 (dd, *J* = 7.9, 1.6 Hz, 1H), 7.70 (dd, *J* = 7.9, 4.8 Hz, 1H), 3.39 (s, 3H).

^{13}C NMR (101 MHz, $CDCl_3$) δ 159.8, 151.8, 143.8, 126.8, 113.2, 107.4, 40.1.

HRMS High accuracy (ASAP): Calculated for $C_7H_6N_2O_2S$ $(M+H)^+$: 183.0228; found: 183.0223.

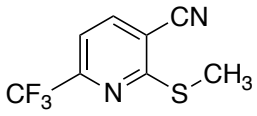

2-(methylthio)-6-(trifluoromethyl)nicotinonitrile (xx-3) The title compound was prepared following the published procedure, the product (yellow solid) was carried towards the synthesis of xx-4 without further purification[41].

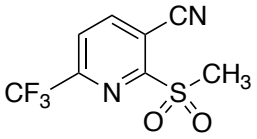

2-(methylsulfonyl)-6-(trifluoromethyl)nicotinonitrile (xx-4) The title compound was prepared from xx-3 according to a modified procedure from the literature[42].

Pyridine xx-2 (105 mg, 0.50 mmol, 1 equiv) was weighed into 50 mL round bottom flask equipped with a stir bar. The solid was dissolved in 10 mL of anhydrous MeOH, followed by portion-wise (usually 3 portions) additions of mCPBA (0.86 mg, 5 mmol, 10 equiv). Substrate conversion was monitored via TLC analysis (40% EtOAc:Hex to 60% EtOAc). Upon complete conversion of starting material, the reaction was quenched with 20 mL of saturated aqueous $NaHCO_3$, diluted with an additional 20 mL of DCM. The layers were separated and the organic layer was further washed (2x) with 10 mL of of saturated aqueous $NaHCO_3$. The organic layer was then dried *in vacuo* and purified via silica gel column chromatography (40% to 80% EtOAc:Hex) to yield 38 mg (30% yield) of the desired sulfone as a white solid.

^{1}H NMR (400 MHz, $CDCl_3$) δ 8.49 (dd, J = 8.1, 0.7 Hz, 1H), 8.06 (d, J = 8.1 Hz, 1H).

^{13}C NMR (101 MHz, $CDCl_3$) δ 160.4, 149.7 (q, J = 37.6 Hz), 146.0, 123.7 (q, J = 2.3 Hz), 120.0 (q, J = 275.5 Hz), 112.1, 109.7, 39.7.

395 ^{19}F NMR (376 MHz, $CDCl_3$) δ -68.28.

396 HRMS High accuracy (ASAP): Calculated for $C_8H_5F_3N_2O_2S$ $(M+H)^+$: 251.0102; found: 251.0104.

397

398 Compound 11a was synthesized according to the specified protocol in Dai. et. al. 2020[26]. Compound

399 11a was confirmed by LCMS with m/z = 453 (M+1) and 451 (M-1).

400

401 Compound 4 was synthesized according to the procedure described in Yang et. al 2006[25]. AZVIII-

402 34D was formed as a byproduct (15%) in the synthesis of Compound 4 and was isolated by RP

403 HPLC. ^{1}H NMR (400 MHz, $CDCl_3$) 7.88 (s, 1H), 7.44-7.34 (m, 5H), 6.80 (d, 1H, J = 15.4 Hz), 6.69 (s,

404 1H), 6.16-5.87 (m, 2H), 5.12 (s, 2H), 4.76 (s, 1H), 4.42 (s, 1H), 4.31-3.99 (m, 4H), 3.39 (s, 2H), 2.40-

405 1.45 (m, 8H), 1.29–1.20 (m, 12H), 1.13-1.02 (m, 3H), 1.00 – 0.89 (m, 6H). MS M+H = 631.

406

407 AZVIII-38, AZVIII-30, and AZVIII-42 were synthesized according the procedures described in Mou

408 et. al. 2008[43]. AZVIII-37A was synthesized as described in Prior et al. 2013. AZVIII-33B was

409 synthesized according to the method described in Amblard et. al. 2018[44].

410

411 AZVIII-41A was synthesized according to the procedure described for synthesizing AZVIII-33B in

412 Amblard et. al. 2018 and substituting Z-Leu-OH for BOC-Leu-OH[44]. ^{1}H NMR (400 MHz, $CDCl_3$) 7.77

413 (s, 1H), 7.41-7.27 (m, 5H), 6.80 (dd, 1H, J = 5.5, 15. 6 Hz), 5.98-5.84 (m, 2H), 5.15-5.03 (m, 2H),

414 4.55 (bd s, 1H), 4.27 (bd s, 1H), 4.23-4.07 (m, 3H), 3.38-3.23 (m, 2H), 2.56–1.40 (m, 8H), 1.33 –

415 1.20 (m, 3H), 0.95 (s, 6H). MS M+H = 474.

416

417 AZVII-43A was synthesized by treatment of a dichloromethane solution of AZVIII-30 and AZVIII-40A

418 with triphenyl phosphine and diethyl azodicarboxylate. ^{1}H NMR (400 MHz, $CDCl_3$) 7.91 (d, 1H, J =

419 8.0), 7.76 (d, 1H, J = 8.0), 7.55-7.34 (m, 2H), 6.16 (bd s, 1H), 5.29 (bd s, 1H), 4.73-4.39 (m, 2H),

420 4.35-3.96 (m, 1H), 3.58-3.16 (m, 2H), 3.79-3.43 (m, 2H), 3.39-3.91 (m, 1H), 1.98-1.77 (m, 1H), 1.73-

421 1.57 (m, 1H), 1.42 (s, 9H). MS M+H = 392.

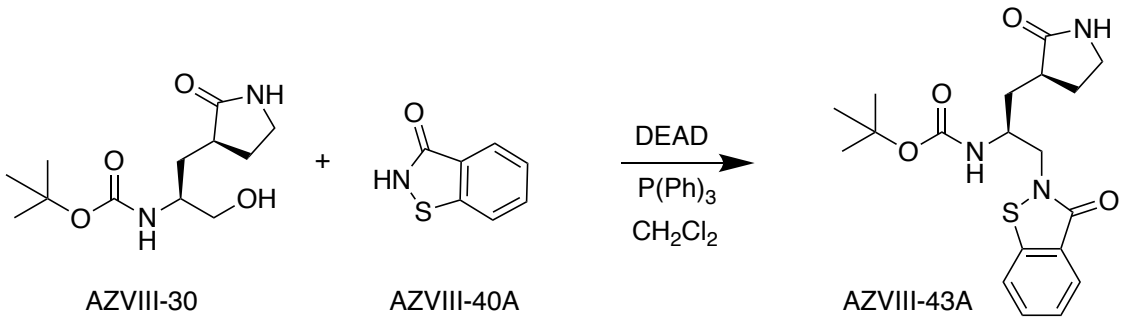

AZVIII-30 AZVIII-40A AZVIII-43A

AZVIII-44B, AZVIII-44D, AZVIII-44E, AZVIII-44H, AZVIII-49C, and AZVIII-49F were synthesized by treatment of the appropriate arylalkylamine or heteroarylalkylamine with the corresponding arylsulfonyl chloride or heteroarylsulfonyl chloride and diisopropylethylamine in dichloromethane. AZVIII-57D was synthesized by treatment of AZVIII-44D with methyl bromoacetate and potassium carbonate in dimethylformamide to give the corresponding ester which was reduced to the corresponding alcohol by treatment with lithium borohydride in tetrahydrofuran. The alcohol was then treated with 1,1,1-tris(acetyloxy)-1,1-dihydro-1,2-benziodoxol-3-(1*H*)-one and sodium bicarbonate in dichloromethane to give to the corresponding aldehyde AZVIII-57D. AZVIII-57G was synthesized from *N*-benzyl-4-methoxybenzenesulfonamide according to the procedure used to synthesize AZVIII-57D.

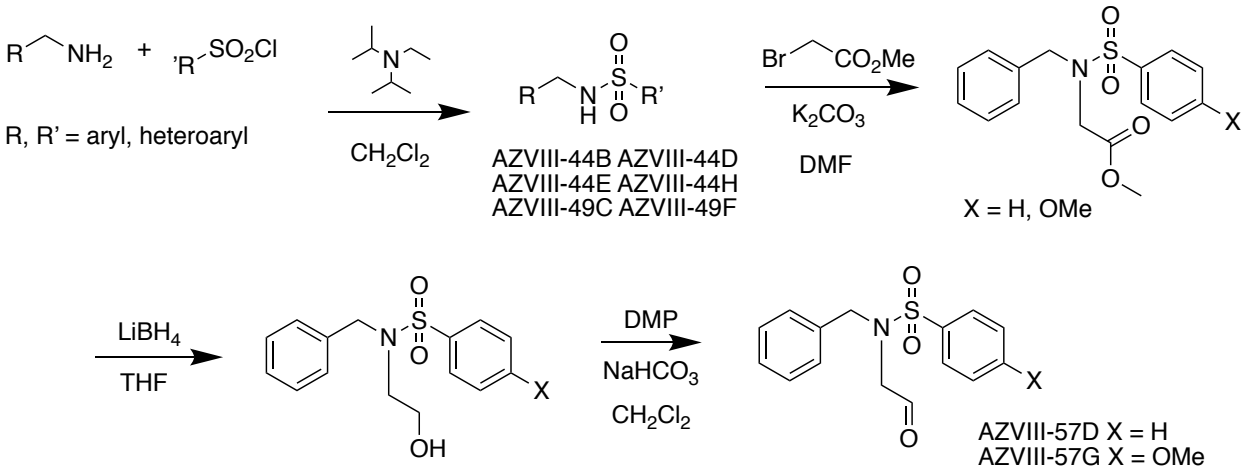

GC373 was synthesized from GC376 by converting the bisulfite group to an aldehyde group by treatment with aqueous sodium bicarbonate. To a solution of 5.31 mg of GC376 in 200 µL H_2O, 2 µL

of saturated $NaHCO_3$ was added. The cloudy mixture was extracted with CH_2Cl_2, dried over Na_2SO_4, and concentrated in vacuo to give GC373 as a colorless oil (4.0 mg).

Data availability

All reagents generated in this study are without restriction. Plasmids generated in this study will be deposited to Addgene. Source data for all figures are provided with this manuscript online. All statistics were performed using Prism v.8.4.2.

Acknowledgements

Compound 11a was synthesized and generously provided by Shi-Xian Deng, Columbia University. This work was supported by a grant from the Jack Ma Foundation to D.D.H. and A.C. and by grants from Columbia Technology Ventures and the Columbia Translational Therapeutics (TRx) program to B.R.S. Further support for these studies comes from a pilot grant award from the Herbert Irving Comprehensive Cancer Center in partnership with the Irving Institute for Clinical and Translational Research at Columbia University to H.Y. and A.C. A.C. is also supported by a Career Awards for Medical Scientists from the Burroughs Wellcome Fund. S.J.R is supported by NIH grant F31NS111851. S.I. is supported by NIH grant T32AI106711.

Author contributions

S.J.R., S.I, and A.C conceived the project. S.J.R., S.I., B.R.S., D.D.H., and A.C. planned and designed the experiments. S.J.R. performed crystal violet-based assays. S.J.R. and S.K. performed the HEK293-EYFP based assays. S.J.R., S.I., and S.J.H. cloned plasmids. A.Z. and H.L. synthesized compounds and provided compound structure information for synthesized compounds. N.E.S.T. and T.R. synthesized compounds NT-1-21, NT-1-24, and NT-1-32. M.S.N. and Y.H. conducted the live virus assays. S.K. and H.Y. performed imaging and created the HEK293-EYFP cell line. S.J.R. and S.M. conducted data analysis. S.J.R, S.I., S.J.H, and A.C. wrote the manuscript with input from all authors.

Competing interests

S.I., H.L., A.Z., B.R.S., A.C., and D.D.H. are inventors on a patent application submitted based on some of the molecules described in this work. B.R.S. is an inventor on additional patents and patent applications related to small molecule therapeutics, and co-founded and serves as a consultant to Inzen Therapeutics and Nevrox Limited.

References

1. Wu, F. *et al.* A new coronavirus associated with human respiratory disease in China. *Nature* **579**, 265–269 (2020).
2. Zhou, P. *et al.* A pneumonia outbreak associated with a new coronavirus of probable bat origin. *Nature* **579**, 270–273 (2020).
3. Pillaiyar, T., Manickam, M., Namasivayam, V., Hayashi, Y. & Jung, S.-H. An Overview of Severe Acute Respiratory Syndrome–Coronavirus (SARS-CoV) 3CL Protease Inhibitors: Peptidomimetics and Small Molecule Chemotherapy. *J. Med. Chem.* **59**, 6595–6628 (2016).
4. de Wit, E., van Doremalen, N., Falzarano, D. & Munster, V. J. SARS and MERS: recent insights into emerging coronaviruses. *Nat. Rev. Microbiol.* **14**, 523–534 (2016).
5. Huang, C., Wei, P., Fan, K., Liu, Y. & Lai, L. 3C-like Proteinase from SARS Coronavirus Catalyzes Substrate Hydrolysis by a General Base Mechanism †. *Biochemistry* **43**, 4568–4574 (2004).
6. Berry, M., Fielding, B. & Gamieldien, J. Human coronavirus OC43 3CL protease and the potential of ML188 as a broad-spectrum lead compound: Homology modelling and molecular dynamic studies. *BMC Struct. Biol.* **15**, (2015).
7. Blanco, R., Carrasco, L. & Ventoso, I. Cell Killing by HIV-1 Protease. *J. Biol. Chem.* **278**, 1086–1093 (2003).
8. Li, H. *et al.* Zika Virus Protease Cleavage of Host Protein Septin-2 Mediates Mitotic Defects in Neural Progenitors. *Neuron* **101**, 1089-1098.e4 (2019).
9. Chau, D. H. W. *et al.* Coxsackievirus B3 proteases 2A and 3C induce apoptotic cell death through mitochondrial injury and cleavage of eIF4GI but not DAP5/p97/NAT1. *Apoptosis* **12**, 513–524 (2007).
10. M'Barek, N. B., Audoly, G., Raoult, D. & Gluschankof, P. HIV-2 Protease resistance defined in yeast cells. *Retrovirology* **3**, 58 (2006).
11. Barco, A., Feduchi, E. & Carrasco, L. Poliovirus Protease 3Cpro Kills Cells by Apoptosis. *Virology* **266**, 352–360 (2000).

12. Li, M.-L. *et al.* The 3C protease activity of enterovirus 71 induces human neural cell apoptosis. *Virology* **293**, 386–395 (2002).
13. Jin, Z. *et al.* Structure of Mpro from SARS-CoV-2 and discovery of its inhibitors. *Nature* **582**, 289–293 (2020).
14. Zhu, W. *et al.* Identification of SARS-CoV-2 3CL Protease Inhibitors by a Quantitative High-throughput Screening. *bioRxiv* 2020.07.17.207019 (2020) doi:10.1101/2020.07.17.207019.
15. CDC. Information for Laboratories about Coronavirus (COVID-19). *Centers for Disease Control and Prevention* https://www.cdc.gov/coronavirus/2019-ncov/lab/lab-biosafety-guidelines.html (2020).
16. Pyrc, K. *et al.* Culturing the Unculturable: Human Coronavirus HKU1 Infects, Replicates, and Produces Progeny Virions in Human Ciliated Airway Epithelial Cell Cultures. *J. Virol.* **84**, 11255–11263 (2010).
17. Sacco, M. D. *et al.* Structure and inhibition of the SARS-CoV-2 main protease reveals strategy for developing dual inhibitors against Mpro and cathepsin L. *bioRxiv* 2020.07.27.223727 (2020) doi:10.1101/2020.07.27.223727.
18. Sies, H. & Parnham, M. J. Potential therapeutic use of ebselen for COVID-19 and other respiratory viral infections. *Free Radic. Biol. Med.* **156**, 107–112 (2020).
19. Feoktistova, M., Geserick, P. & Leverkus, M. Crystal Violet Assay for Determining Viability of Cultured Cells. *Cold Spring Harb. Protoc.* **2016**, pdb.prot087379 (2016).
20. Ma, C. *et al.* Boceprevir, GC-376, and calpain inhibitors II, XII inhibit SARS-CoV-2 viral replication by targeting the viral main protease. *Cell Res.* 1–15 (2020) doi:10.1038/s41422-020-0356-z.
21. Vuong, W. *et al.* Feline coronavirus drug inhibits the main protease of SARS-CoV-2 and blocks virus replication. *bioRxiv* 2020.05.03.073080 (2020) doi:10.1101/2020.05.03.073080.
22. Froggatt, H. M., Heaton, B. E. & Heaton, N. S. Development of a fluorescence based, high-throughput SARS-CoV-2 $3CL^{pro}$ reporter assay. *bioRxiv* 2020.06.24.169565 (2020) doi:10.1101/2020.06.24.169565.

23. Luan, X. *et al.* Structure Basis for Inhibition of SARS-CoV-2 by the Feline Drug GC376. *bioRxiv* 2020.06.07.138677 (2020) doi:10.1101/2020.06.07.138677.

24. Iketani, S. *et al.* Lead compounds for the development of SARS-CoV-2 3CL protease inhibitors. *bioRxiv* 2020.08.03.235291 (2020) doi:10.1101/2020.08.03.235291.

25. Yang, S. *et al.* Synthesis, Crystal Structure, Structure−Activity Relationships, and Antiviral Activity of a Potent SARS Coronavirus 3CL Protease Inhibitor. *J. Med. Chem.* **49**, 4971–4980 (2006).

26. Dai, W. *et al.* Structure-based design of antiviral drug candidates targeting the SARS-CoV-2 main protease. *Science* **368**, 1331–1335 (2020).

27. Ghosh, A. K. *et al.* Design, synthesis and antiviral efficacy of a series of potent chloropyridyl ester-derived SARS-CoV 3CLpro inhibitors. *Bioorg. Med. Chem. Lett.* **18**, 5684–5688 (2008).

28. Węglarz-Tomczak, E., Tomczak, J. M., Talma, M. & Brul, S. Ebselen as a highly active inhibitor of PL^{Pro}CoV2. *bioRxiv* 2020.05.17.100768 (2020) doi:10.1101/2020.05.17.100768.

29. Seale, L. A., Torres, D. J., Berry, M. J. & Pitts, M. W. A role for selenium-dependent GPX1 in SARS-CoV-2 virulence. *Am. J. Clin. Nutr.* doi:10.1093/ajcn/nqaa177.

30. Kim, Y. *et al.* Reversal of the Progression of Fatal Coronavirus Infection in Cats by a Broad-Spectrum Coronavirus Protease Inhibitor. *PLOS Pathog.* **12**, e1005531 (2016).

31. Zhang, J.-H., Chung, T. D. Y. & Oldenburg, K. R. A Simple Statistical Parameter for Use in Evaluation and Validation of High Throughput Screening Assays. *J. Biomol. Screen.* **4**, 67–73 (1999).

32. Birmingham, A. *et al.* Statistical Methods for Analysis of High-Throughput RNA Interference Screens. *Nat. Methods* **6**, 569–575 (2009).

33. Kim, Y. *et al.* Broad-Spectrum Antivirals against 3C or 3C-Like Proteases of Picornaviruses, Noroviruses, and Coronaviruses. *J. Virol.* **86**, 11754–11762 (2012).

34. Blanchard, J. E. *et al.* High-throughput screening identifies inhibitors of the SARS coronavirus main proteinase. *Chem. Biol.* **11**, 1445–1453 (2004).

549 35. Klotz, L. C. & Sylvester, E. J. The Consequences of a Lab Escape of a Potential Pandemic
550 Pathogen. *Front. Public Health* **2**, (2014).
551 36. Coelho, A. C. & García Díez, J. Biological Risks and Laboratory-Acquired Infections: A Reality
552 That Cannot be Ignored in Health Biotechnology. *Front. Bioeng. Biotechnol.* **3**, (2015).
553 37. Tan, C. W. *et al.* A SARS-CoV-2 surrogate virus neutralization test based on antibody-mediated
554 blockage of ACE2–spike protein–protein interaction. *Nat. Biotechnol.* (2020)
555 doi:10.1038/s41587-020-0631-z.
556 38. Case, J. B. *et al.* Neutralizing Antibody and Soluble ACE2 Inhibition of a Replication-Competent
557 VSV-SARS-CoV-2 and a Clinical Isolate of SARS-CoV-2. *Cell Host Microbe*
558 doi:10.1016/j.chom.2020.06.021.
559 39. Dieterle, M. E. *et al.* A Replication-Competent Vesicular Stomatitis Virus for Studies of SARS-
560 CoV-2 Spike-Mediated Cell Entry and Its Inhibition. *Cell Host Microbe*
561 doi:10.1016/j.chom.2020.06.020.
562 40. Iglewicz, B. & Hoaglin, D. C. *How to detect and handle outliers*. (ASQC Quality Press, 1993).
563 41. Metzger, A., Melzig, L., Despotopoulou, C. & Knochel, P. Pd-Catalyzed Cross-Coupling of
564 Functionalized Organozinc Reagents with Thiomethyl-Substituted Heterocycles. *Org. Lett.* **11**,
565 4228–4231 (2009).
566 42. Zambaldo, C. *et al.* 2-Sulfonylpyridines as Tunable, Cysteine-Reactive Electrophiles. *J. Am.*
567 *Chem. Soc.* **142**, 8972–8979 (2020).
568 43. Mou, K. *et al.* Novel CADD-based peptidyl vinyl ester derivatives as potential proteasome
569 inhibitors. *Bioorg. Med. Chem. Lett.* **18**, 2198–2202 (2008).
570 44. Amblard, F. *et al.* Synthesis and antiviral evaluation of novel peptidomimetics as norovirus
571 protease inhibitors. *Bioorg. Med. Chem. Lett.* **28**, 2165–2170 (2018).

572 **Fig. 1. Expression of SARS-CoV-2 3CLpro in HEK293T cells results in toxicity that can be**
573 **rescued by GC376. a**. SARS-CoV-2 3CL toxicity is dependent on protease activity and can be
574 visualized with crystal violet staining. **b**. Quantification of crystal violet staining in a. **c**. Treatment of
575 SARS-CoV-2 3CLpro expressing cells with protease inhibitor GC376 results in rescue of cytotoxicity.
576 **d**. Quantification of c. Data are shown as mean ± s.d. for four technical replicates.

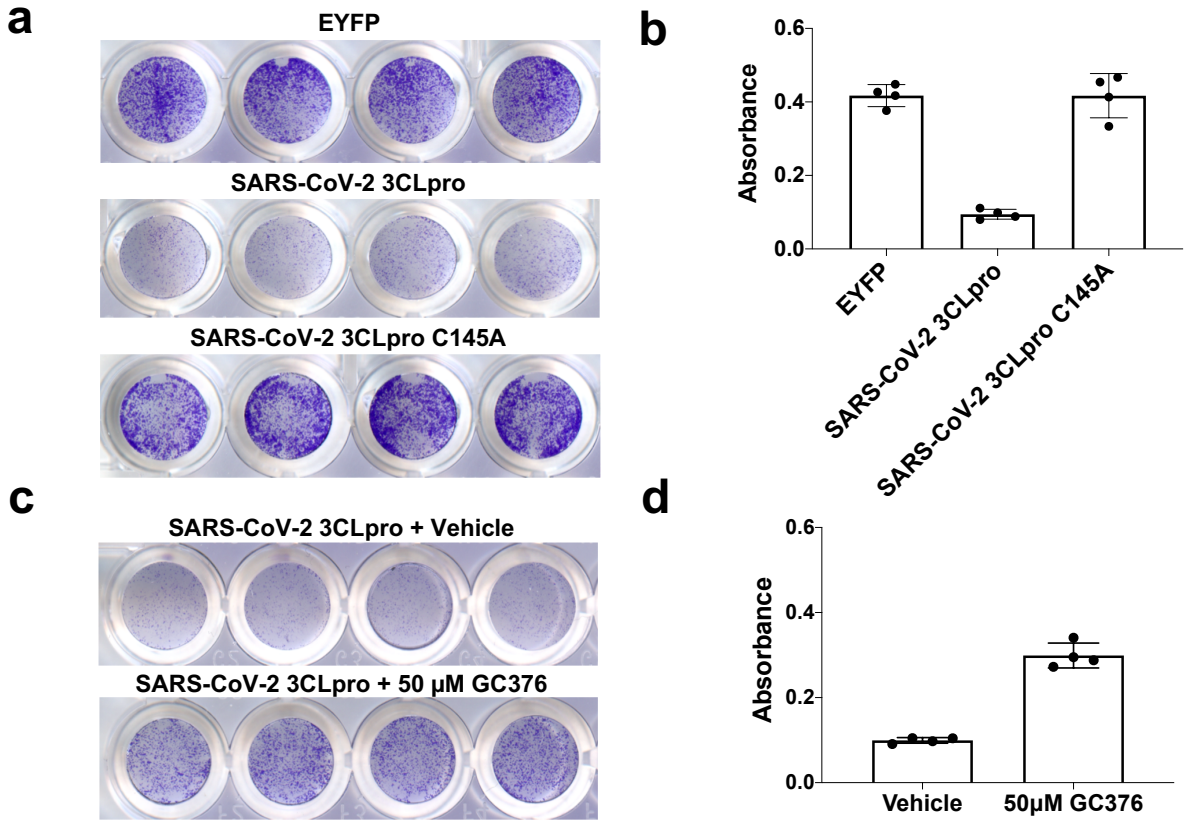

577

578 **Fig. 2. Dose response curves for SARS-CoV-2 3CLpro can be conducted with transfection-**
579 **based assays. a-c**. SARS-CoV-2 3CLpro can be inhibited by known 3CLpro inhibitors GC376,
580 compound 4, and 11a. The toxicity of each compound was determined by treating EYFP-transfected
581 cells with indicated concentrations of drug and is reported as Cell Viability. **d.** Chemical structures for
582 each of the compounds tested. EC_{50} values are displayed as best-fit value alongside 95%
583 confidence interval. CC_{50} values are displayed as best-fit value. Data are shown as mean ± s.d. for
584 four technical replicates.

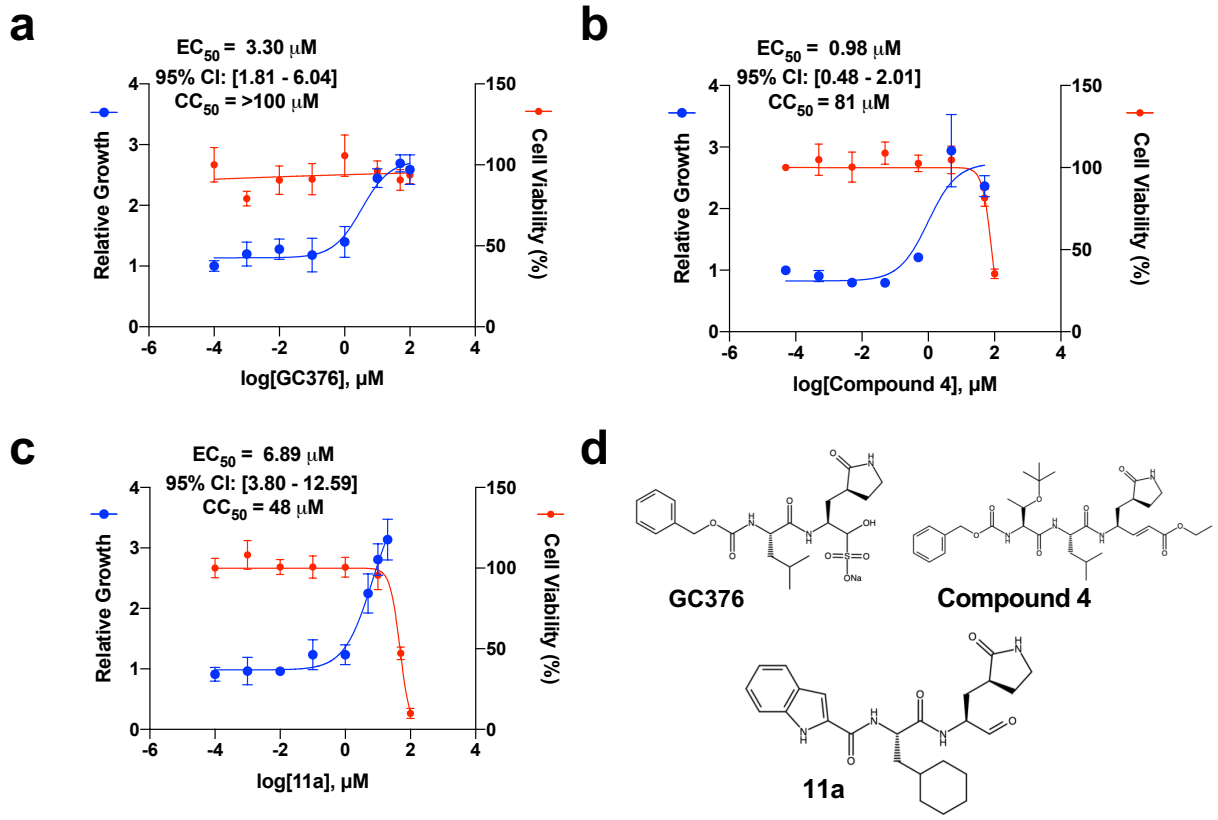

585

586 **Fig. 3. The activity of GC376, compound 4, and 11a show variable effectiveness and potency**
587 **against the coronavirus 3CL proteases from SARS-CoV, MERS-CoV, Bat-CoV-HKU9, HCoV-**
588 **NL63, and IBV.** EC_{50} values are displayed as best-fit value alongside 95% confidence interval. CC_{50}
589 values are displayed as best-fit value. Data are shown as mean ± s.d. for three or four technical
590 replicates.

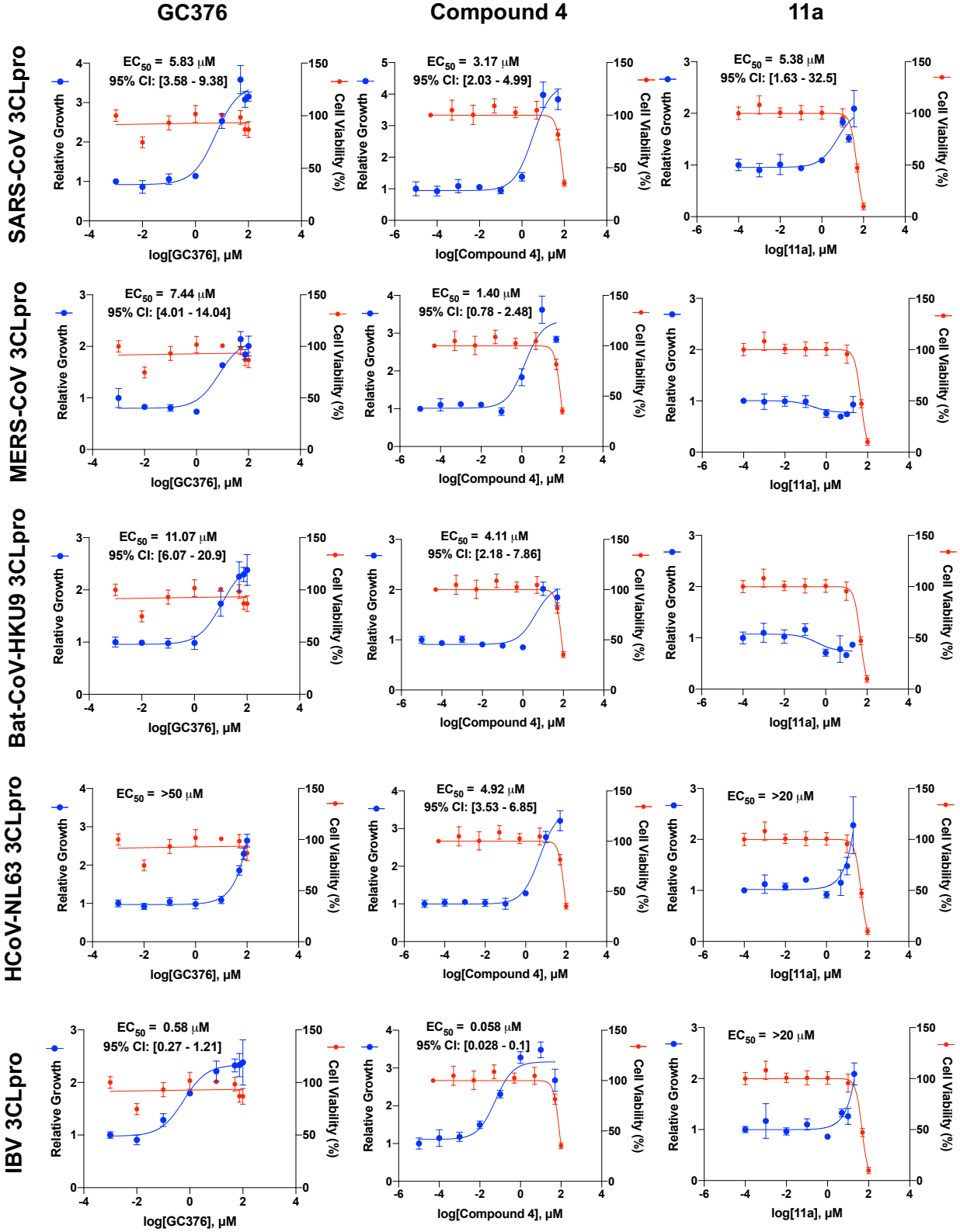

591

Fig. 4. Small-scale drug screen and structure-activity profiling at 10 μM identify two compounds, GC373 and GRL-0496, with activity against the SARS-CoV-2 3CLpro. a. Identification of hits from the drug screen and structure-activity profiling. Positive control compounds were included in each plate and are highlighted. **b**. Compounds with structural similarity to known inhibitors. Compounds in bold are molecules that show activity against the SARS-CoV-2 3CLpro at 10 μM. **c**. Dose-response profiling and cytotoxicity determination of GRL-0496 against the SARS-CoV-2 3CLpro. **d**. Live virus testing of GRL-0496 against SARS-CoV-2.
EC_{50} values are displayed as best-fit value alongside 95% confidence interval. The live virus assay was conducted with two biological replicates, each with three technical replicates and the EC_{50} value was derived from all replicates. CC_{50} values are displayed as best-fit value. Data are shown as mean ± s.d. for three or four technical replicates.

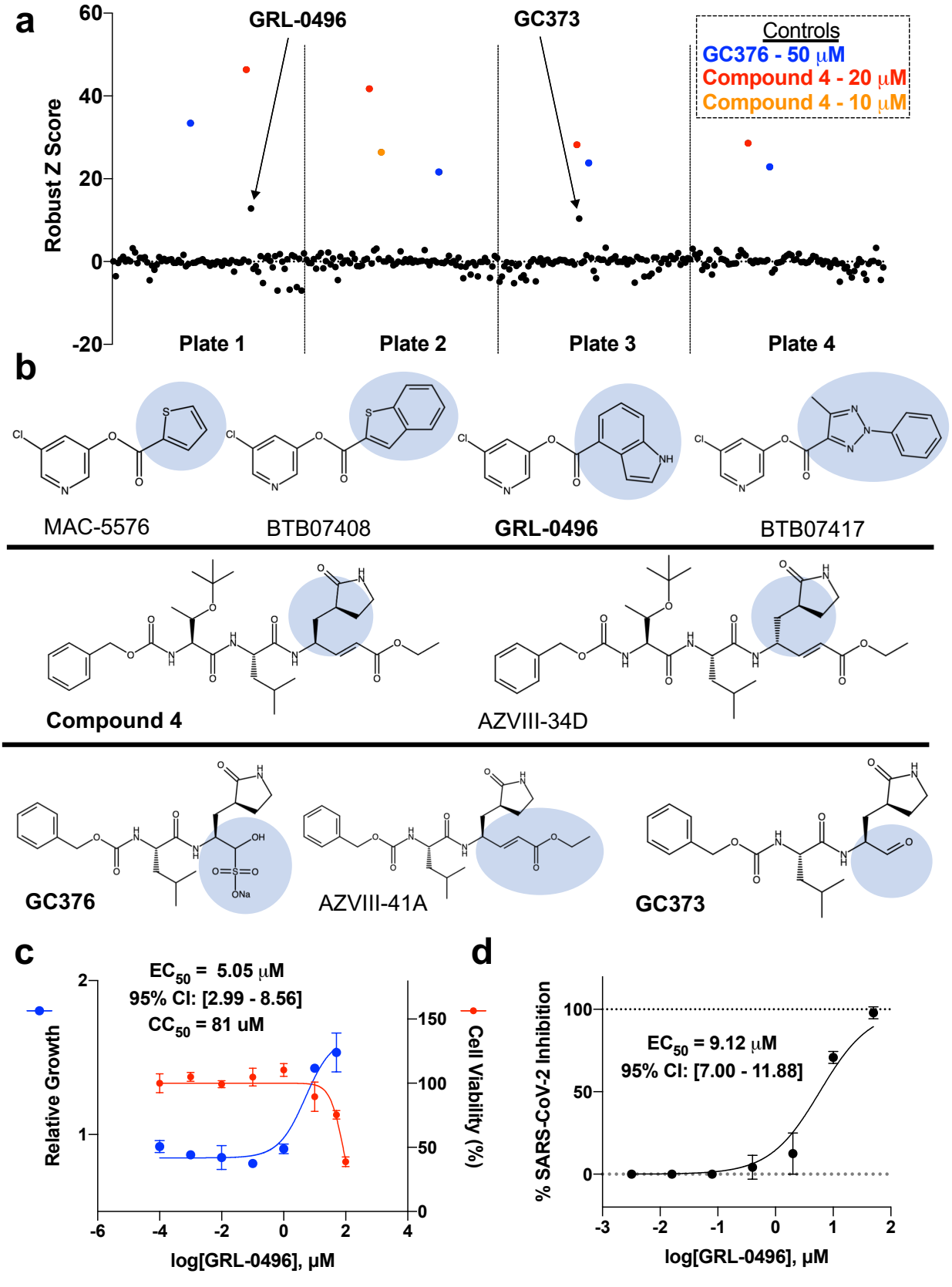

603

604 **Table 1. Comparison of literature reported live virus based EC_{50} values compared to values**

605 **generated during this study.** CPE = Cytopathic effect.

Protease	Drug	Calculated EC_{50} (μM)	Literature Reported Value (μM)	Method	Cell Line	Citation
SARS-CoV-2 3CLpro	GC376	3.3	3.37	CPE	Vero 76	Ma et. al.
			0.9	Plaque Assay	Vero E6	Vuong et. al.
			0.18	qPCR	Vero E6	Luan et. al.
			2.2	qPCR	Vero E6	Froggatt et. al.
			4.48	CPE	Vero E6	Iketani et. al.
SARS-CoV-2 3CLpro	11a	6.89	2.06	CPE	Vero E6	This study
			0.53	Plaque Assay	Vero E6	Dai et. al.
SARS-CoV-2 3CLpro	Compound 4	0.98	3.023	CPE	Vero E6	Iketani et. al.
SARS-CoV-2 3CLpro	GRL-0496	5.05	9.12	CPE	Vero E6	This study
SARS-CoV 3CLpro	GRL-0496	7.84	6.9	CPE	Vero E6	Ghosh et. al.
SARS-CoV-2 3CLpro	GC373	2.8	1.5	Plaque Assay	Vero E6	Vuong et. al.
			4.83	CPE	Vero E6	This Study

606